The Astrophysical Journal, 662:236–249, 2007 June 10

SEARCHING FOR ROTATING GALAXY CLUSTERS IN SDSS AND 2dFGRS

Ho Seong Hwang and Myung Gyoon Lee
Astronomy Program, Department of Physics and Astronomy, Seoul National University, Seoul 151-742, Korea;
hshwang@astro.snu.ac.kr, mglee@astrog.snu.ac.kr
Received 2006 November 15; accepted 2007 February 6

ABSTRACT

We present the results of a search for galaxy clusters that show an indication of global rotation using a spectroscopic sample of galaxies in SDSS and 2dFGRS. We have determined the member galaxies of 899 Abell clusters covered by these surveys using the galaxies' redshift and positional data and have estimated the ratio of the cluster rotation amplitude to the cluster velocity dispersion and the velocity gradient across the cluster. We found 12 tentative rotating clusters with large ratios of rotation amplitude to dispersion and large velocity gradients. We determine the morphological parameters for these 12 clusters using the positional information on the member galaxies: the ellipticity of the dispersion ellipse is in the range 0.08–0.57, and the position angle of its major and minor axes does not appear to be related to that of the rotation axis. We investigate the substructures in the sample of tentative rotating clusters, finding from Dressler-Shectman plots that the majority (9 out of 12) show evidence of substructure due to spatially correlated galaxy velocities. We have selected six probable rotating clusters (Abell 954, 1139, 1399, 2162, 2169, and 2366) that show a single number-density peak around the cluster center with a spatial segregation of high- and low-velocity galaxies. We find no strong evidence of recent mergers for the probable rotating clusters: they do not deviate significantly from the relation between X-ray luminosity and the velocity dispersion or virial mass of the clusters, and in two (Abell 954 and Abell 1399), the brightest cluster galaxies have small values of peculiar velocity and clustercentric distance.

Subject headings: galaxies: clusters: general — galaxies: kinematics and dynamics

Online material: color figures

1. INTRODUCTION

Global rotation has been suggested to exist in several galaxy clusters (e.g., Materne & Hopp 1983; Oegerle & Hill 1992; Dupke & Bregman 2001b), but there is still no conclusive evidence of cluster rotation. There are two kinds of objects to consider in this regard: the intracluster medium (ICM) and the galaxies themselves.

For the ICM, recent studies have searched for bulk motions or a velocity gradient in several clusters using data from the *Advanced Satellite for Cosmology and Astrophysics* (*ASCA*) and from *Chandra*. Dupke & Bregman (2001a, 2001b) directly detected, for the first time, ICM bulk motions in the outer regions of the Centaurus (Abell 3526) and Perseus (Abell 426) clusters using *ASCA* data. Later, Dupke & Bregman (2005) identified two more clusters (Abell 576 and RX J0419.5+0225) that had the most significant velocity gradients among 12 clusters for which velocity mapping could be performed with useful precision in the *ASCA* archive. Recently, Dupke & Bregman (2006) measured a velocity difference of $(2.4 \pm 1.0) \times 10^3$ km s^{-1} for opposing regions around the center of the ICM in the Centaurus Cluster using *Chandra* data. If this velocity difference is due to the circulation of gas around the cluster center, then the corresponding circular velocity would be as large as $(1.2 \pm 0.7) \times 10^3$ km s^{-1}.

For galaxies in clusters, global velocity gradients suggestive of cluster rotation have been detected in some cases (Materne & Hopp 1983; Biviano et al. 1996; den Hartog & Katgert 1996; Burgett et al. 2004). Den Hartog & Katgert (1996) found 13 clusters that showed significant velocity gradients, in the range 240–1230 km s^{-1} Mpc^{-1}, among 72 clusters. Burgett et al. (2004) reported three clusters (Abell 1139, 1663, and S333) that exhibit velocity-position characteristics consistent with the presence of possible cluster rotation, shear, or infall dynamics. Up to now, there has been only one galaxy cluster for which the global rotation of galaxies was studied in detail: Abell 2107. Oegerle & Hill (1992) found from an analysis of 75 member galaxies that Abell 2107 appears to be a regular cluster (single-peaked galaxy distribution, regular X-ray morphology, and Gaussian velocity histogram) but has spatially correlated velocities of galaxies (high- and low-velocity galaxies are segregated spatially). They concluded that the spatial distribution of the galaxy velocities is consistent with the rotation of a single cluster at the 98% confidence level. Recently, Kalinkov et al. (2005) suggested that the virial mass of Abell 2107, as determined in their study, should be corrected from $(3.2 \pm 0.6) \times 10^{14}\ M_\odot$ to $(2.8 \pm 0.5) \times 10^{14}\ M_\odot$ because of the cluster rotation.

Theoretically, a galaxy cluster is expected to acquire angular momentum through an off-axis merger or from global rotation of the universe. First, off-axis merging between two clusters is expected to provide angular momentum to the clusters, resulting in rotating clusters (Ricker 1998; Takizawa 2000; Ricker & Sarazin 2001; Pawl et al. 2005). According to models of this process, the global rotation of the "collisional" ICM that originates in mergers survives longer than that of "collisionless" galaxies in clusters (Roettiger & Flores 2000). Therefore, it is expected to be more difficult to detect the global rotation of galaxies than that of the ICM. Second, global rotation of the universe may provide angular momentum to celestial bodies upon their formation, resulting in rotating systems (Li 1998). The Li model explains the empirical relation between the angular momenta and the masses of galaxies. Later, Godłowski et al. (2003) showed that the Li model predicts the presence of a minimum (i.e., vanishing angular momentum) in the relation between the angular momenta and the masses of celestial bodies. This prediction was observationally tested (Godłowski et al. 2005); vanishing angular momenta for the masses corresponding to galaxy groups and nonvanishing angular

momenta for smaller and larger structures (compact groups and rich galaxy clusters) were found. However, the nonvanishing angular momenta for galaxy clusters were found indirectly, based on the study of the galaxy orientations. Therefore, it is necessary to probe the angular momenta of galaxy clusters directly based on dynamical analysis.

Recently, galaxy redshift surveys such as the Sloan Digital Sky Survey (SDSS; York et al. 2000) and the 2dF Galaxy Redshift Survey (2dFGRS; Colless et al. 2001) have provided redshift data for large samples of galaxies. By identifying member galaxies in clusters using these redshift and positional data, we can search for the global rotation of galaxies in clusters for a large sample of galaxy clusters.

In this paper, we present the result of such a search for galaxy clusters that show an indication of global rotation, using a spectroscopic sample of galaxies in SDSS and 2dFGRS. Section 2 describes the galaxy sample and the cluster sample. The algorithm for identifying tentative rotating clusters and the results are presented in § 3. Analysis of the cluster morphology and substructure for tentative rotating clusters is given in § 4. A detailed analysis of the individual clusters is presented in § 5. We discuss the properties of the probable rotating clusters in § 6. A summary of this study is given in the final section. Throughout, we adopt cosmological parameters $h = 0.7$, $\Omega_\Lambda = 0.7$, and $\Omega_M = 0.3$.

2. DATA

We used data from the spectroscopic sample of galaxies in the SDSS Fifth Data Release[1] and in the 2dFGRS Final Data Release (Colless et al. 2001). SDSS Data Release 5 contains five-band (*ugriz*) photometric data for 215 million objects over 8000 deg^2 and optical spectroscopic data for 1 million galaxies, quasars, and stars over 5740 deg^2. We used the spectroscopic sample of 674,000 galaxies for this study. The median redshift for this spectroscopic sample is 0.11. The redshifts were measured from the spectra, covering 3800–9200 Å, with an uncertainty of $\sim$30 km s^{-1}. A redshift confidence parameter (zConf) is assigned from 0 to 1 in the SDSS catalogs. We used only those galaxies with zConf $\geq$ 0.65.

The 2dFGRS contains spectra for nearly 246,000 galaxies selected in the photographic b_J band from the APM galaxy catalog. The survey covers over 2000 deg^2, and the median redshift for the sample of galaxies is similar to that of SDSS. The redshift measurements are from spectra covering 3600–8000 Å, and a redshift quality parameter Q is assigned in the range 1–5. The redshift measurements with $Q \geq 3$ are 98.4% reliable and have an overall rms uncertainty of $\sim$85 km s^{-1}. We used only the galaxies with $Q \geq 3$ in this study.

Since some galaxies are covered in both SDSS and 2dFGRS, we matched the galaxies found in SDSS with those in 2dFGRS to make a master catalog. The mean difference in radial velocity Δv ($=v_{\rm SDSS} - v_{\rm 2dFGRS}$) between the SDSS and 2dFGRS measurements for the 31,300 matched galaxies is $\sim$13 km s^{-1}. We corrected the SDSS velocities by this mean difference and used the average value of the velocities measured in SDSS and in 2dFGRS for further analysis.

We used the Abell catalog of galaxy clusters (Abell et al. 1989) to find the clusters in the survey data. Among the Abell clusters, we selected those that have known spectroscopic redshifts in the NASA/IPAC Extragalactic Database (NED). Finally, we selected 899 clusters located within the survey regions of SDSS and 2dFGRS as a sample for further analysis.

[1] The details of Data Release 5 can be found on the SDSS Web site (http://www.sdss.org/dr5).

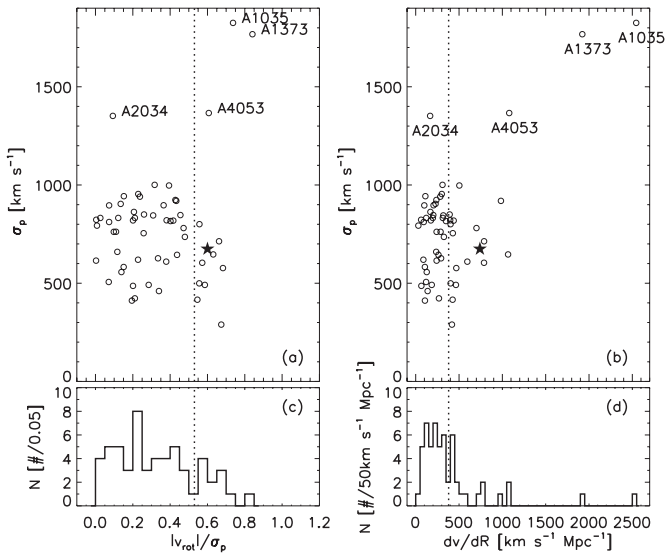

FIG. 1.—Velocity dispersions of galaxy clusters vs. (*a*) ratio of the absolute value of rotation amplitude to the velocity dispersion and (*b*) the global velocity gradient. Histograms for the ratios and velocity gradients are shown in (*c*) and (*d*), respectively. The dotted vertical lines indicate the adopted selection criteria for the tentative rotating cluster candidates. Stars represent A2107, known as a probable rotating cluster.

3. IDENTIFICATION OF CANDIDATE ROTATING CLUSTERS

We applied the following procedure to identify the rotating-cluster candidates in SDSS and 2dFGRS:

1. In order to select member galaxies in the target clusters, we used the "shifting gapper" method of Fadda et al. (1996). In a plot of radial velocity versus clustercentric distance of galaxies for a given cluster, we selected galaxies as cluster members using a velocity gap of 950 km s^{-1} and a distance bin of 0.2 Mpc shifting along the distance from the cluster center. We used a larger bin width if the number of galaxies in a bin was less than 15. We applied this method to the galaxies within the radius at which the distance between adjacent galaxies is larger than 0.1 Mpc. We iterated the procedure until the number of cluster members stabilized. Finally, we selected 56 galaxy clusters in which the number of member galaxies is greater than or equal to 40 for further analysis.

2. To investigate the global rotation of the clusters, we fitted the observed radial velocities v_p of the cluster galaxies with a function of position angle,

$$v_p(\Theta) = v_{\rm sys} + v_{\rm rot} \sin(\Theta - \Theta_0), \quad (1)$$

where Θ is the projected position angle of a galaxy relative to the cluster center (measured from north to east), Θ_0 is the projected position angle of the rotation axis of the cluster, $v_{\rm rot}$ is the rotation amplitude, and $v_{\rm sys}$ is the systemic velocity of the galaxy cluster.

Similarly, the effect of the global rotation of galaxy clusters can appear as a velocity gradient across the cluster. To investigate the global velocity gradient, we fitted the observed radial velocities of the cluster galaxies with a function of position on the plane of the sky,

$$v_p(X, Y) = v_{\rm sys} + \frac{\partial v}{\partial X} X + \frac{\partial v}{\partial Y} Y, \quad (2)$$

TABLE 1
THE SAMPLE OF TENTATIVE ROTATING CLUSTERS

Cluster	R.A. (J2000)	Decl. (J2000)	B-M Type	$\overline{cz}$ (km s^{-1})	σ_p (km s^{-1})	N_{gal}	L_X(0.1–2.4 keV)[a] (10^{44} ergs cm^{-2} s^{-1})	X-Ray Reference
S1171	00 01 21.70	−27 32 18.0	II	8377^{+178}_{-117}	646^{+168}_{-166}	42	...	
S0001	00 02 33.93	−30 44 06.2	I	8815^{+142}_{-128}	577^{+71}_{-99}	51	...	
A954	10 13 44.81	−00 06 31.0	...	28459^{+108}_{-98}	801^{+64}_{-59}	67	0.70	1
A1035	10 32 14.16	40 14 49.2	II–III	21753^{+188}_{-208}	1825^{+82}_{-81}	97	0.92	2, 3
A1139	10 58 10.39	01 35 11.0	III	11849^{+48}_{-45}	491^{+37}_{-36}	122	0.09	1, 2, 3, 4
A1373	11 45 30.95	−02 27 12.9	III	37595^{+317}_{-261}	1768^{+120}_{-124}	48	...	
A1399	11 51 10.78	−03 01 41.3	III	27267^{+48}_{-46}	289^{+41}_{-39}	41	...	
A1474	12 07 57.20	14 57 18.0	III	24151^{+105}_{-101}	714^{+49}_{-45}	60	0.03	3
A2162	16 12 30.00	29 32 23.0	II–III	9653^{+68}_{-64}	416^{+33}_{-32}	41	0.01	3
A2169	16 14 09.60	49 09 10.8	III	17343^{+63}_{-58}	499^{+39}_{-39}	71	0.45	2, 3
A2366	21 42 50.41	−06 52 15.0	I–II	15914^{+103}_{-95}	604^{+56}_{-53}	41	0.05	3
A4053	23 54 45.39	−27 40 52.8	III	20691^{+203}_{-184}	1366^{+149}_{-143}	76	...	

NOTE.—Units of right ascension are hours, minutes, and seconds, and units of declination are degrees, arcminutes, and arcseconds.
[a] X-ray luminosities from Ledlow et al. (2003) are in the 0.5–2.0 keV band.
REFERENCES.—(1) Böhringer et al. 2004; (2) Ebeling et al. 2000; (3) Ledlow et al. 2003; (4) Böhringer et al. 2000.

where X and Y are clustercentric distances in the direction of right ascension and declination, respectively. We fitted the observed radial velocities of cluster galaxies using equations (1) and (2), with v_{sys} as a fixed value of the mean radial velocity of cluster galaxies (the biweight location of Beers et al. 1990).

In Figure 1, we plot the velocity dispersions (the biweight scale of Beers et al. 1990) of galaxy clusters as a function of $|v_{rot}|/\sigma_p$, the ratio of the absolute value of the rotation amplitude to the velocity dispersion (*left*), and as a function of $dv/dr \equiv [(\partial v/\partial X)^2 + (\partial v/\partial Y)^2]^{1/2}$, the global velocity gradient (*right*). Figure 1 shows that there are four clusters (A1035, A1373, A2034, and A4053) that have unusually large velocity dispersions (>1300 km s^{-1}), while the majority of clusters lie in the range 290 km s^{-1} $< \sigma_p <$ 1050 km s^{-1}. The large velocity dispersions of these four clusters might be related to the superposition or interaction of two clusters with slightly different systemic velocities (discussed in § 5).

It is expected that a rotating cluster will have a large ratio of the absolute value of rotation amplitude to the velocity dispersion $|v_{rot}|/\sigma_p$ and exhibit a large global velocity gradient dv/dR across the cluster. Therefore, among the 56 selected galaxy clusters, we selected 12 tentative rotating clusters for which $|v_{rot}|/\sigma_p$ is greater than 0.53 and dv/dR is greater than 380 km s^{-1} Mpc^{-1}. We chose these critical values because the estimated values of the rotation amplitudes of the clusters that lie above these values are larger than $\sim 2\,\sigma$. In addition, dips are seen at the critical values in both Figures 1*c* and 1*d*, implying that a segregation between the rotating and nonrotating clusters might exist, although it is not known whether or not there is a discrete boundary in rotation amplitude between the rotating and nonrotating clusters. These selection criteria are represented by dotted vertical lines in Figure 1. For comparison, we also plot the data for Abell 2107 (*stars*), which is known probably to be rotating (Oegerle & Hill 1992; Kalinkov et al. 2005). It can be seen that Abell 2107 also satisfies our selection criteria for tentative rotating clusters.

Table 1 lists the tentative rotating clusters with Abell identification, right ascension and declination, Bautz-Morgan (B-M) type, the redshift derived in this study, the velocity dispersion derived in this study, the number of member galaxies, the X-ray luminosity, and references for the latter. The sample of tentative rotating clusters are found from $z = 0.028$ to $z = 0.125$ and have 41–122 member galaxies. There are seven clusters for which X-ray luminosities have been estimated, and six clusters of Bautz-Morgan type III.

The rotational properties derived using equations (1) and (2) are summarized in Table 2. The first column gives the Abell identification. The second and third columns represent, respectively, the position angle of the rotation axis and the rotation amplitude derived using equation (1). The ratio of the absolute value of the rotation amplitude to the velocity dispersion, $|v_{rot}|/\sigma_p$, is shown in the fourth column. The fifth column gives the position angle defined by $\Theta_1 = \tan^{-1}[(\partial v/\partial Y)/(\partial v/\partial X)] - \pi/2$. The final column gives the global velocity gradient derived using equation (2). The uncertainties on these values represent 68% (1 σ) confidence intervals. We computed the uncertainties using 1000 artificial data sets constructed by randomly choosing cluster galaxies up to the number of cluster members in the real data. The fitting procedure is performed on the 1000 trial data sets, the results are sorted, and the values corresponding to the 16th and the 84th percentiles are identified. The uncertainties are defined as the offsets between these values and the values computed using the real data. In Table 2, there are two clusters (A1035 and A1373) that have unusually large rotation amplitudes (>1300 km s^{-1}) and velocity gradients (>1900 km s^{-1} Mpc^{-1}), due to the superposition of two disparate groups (discussed in § 5). The other

TABLE 2
KINEMATIC PROPERTIES OF THE TENTATIVE ROTATING CLUSTERS

Cluster	Θ_0 (deg)	v_{rot} (km s^{-1})	$\lvert v_{rot}\rvert/\sigma_p$	Θ_1 (deg)	dv/dR (km s^{-1} Mpc^{-1})
S1171	11^{+22}_{-24}	408^{+135}_{-124}	$0.63^{+0.17}_{-0.14}$	1^{+19}_{-23}	1066^{+229}_{-206}
S0001	173^{+13}_{-15}	394^{+83}_{-78}	$0.68^{+0.12}_{-0.10}$	144^{+25}_{-19}	468^{+138}_{-120}
A954	103^{+13}_{-17}	446^{+145}_{-133}	$0.56^{+0.18}_{-0.16}$	100^{+14}_{-27}	402^{+185}_{-162}
A1035	268^{+11}_{-9}	1345^{+184}_{-177}	$0.74^{+0.09}_{-0.09}$	264^{+10}_{-9}	2545^{+414}_{-394}
A1139	37^{+13}_{-11}	288^{+52}_{-48}	$0.59^{+0.10}_{-0.10}$	40^{+9}_{-9}	464^{+65}_{-63}
A1373	155^{+11}_{-12}	1486^{+290}_{-262}	$0.84^{+0.15}_{-0.13}$	149^{+15}_{-17}	1923^{+448}_{-345}
A1399	207^{+27}_{-19}	195^{+62}_{-58}	$0.67^{+0.15}_{-0.14}$	186^{+29}_{-14}	418^{+151}_{-108}
A1474	268^{+15}_{-11}	472^{+129}_{-120}	$0.66^{+0.16}_{-0.16}$	262^{+8}_{-8}	789^{+193}_{-175}
A2162	359^{+20}_{-20}	227^{+80}_{-76}	$0.55^{+0.18}_{-0.17}$	351^{+25}_{-32}	426^{+177}_{-155}
A2169	342^{+19}_{-22}	277^{+61}_{-61}	$0.56^{+0.11}_{-0.11}$	23^{+13}_{-16}	403^{+124}_{-101}
A2366	309^{+19}_{-17}	346^{+147}_{-142}	$0.57^{+0.21}_{-0.22}$	300^{+19}_{-30}	788^{+376}_{-327}
A4053	282^{+14}_{-16}	829^{+204}_{-181}	$0.61^{+0.12}_{-0.12}$	269^{+15}_{-12}	1079^{+217}_{-185}

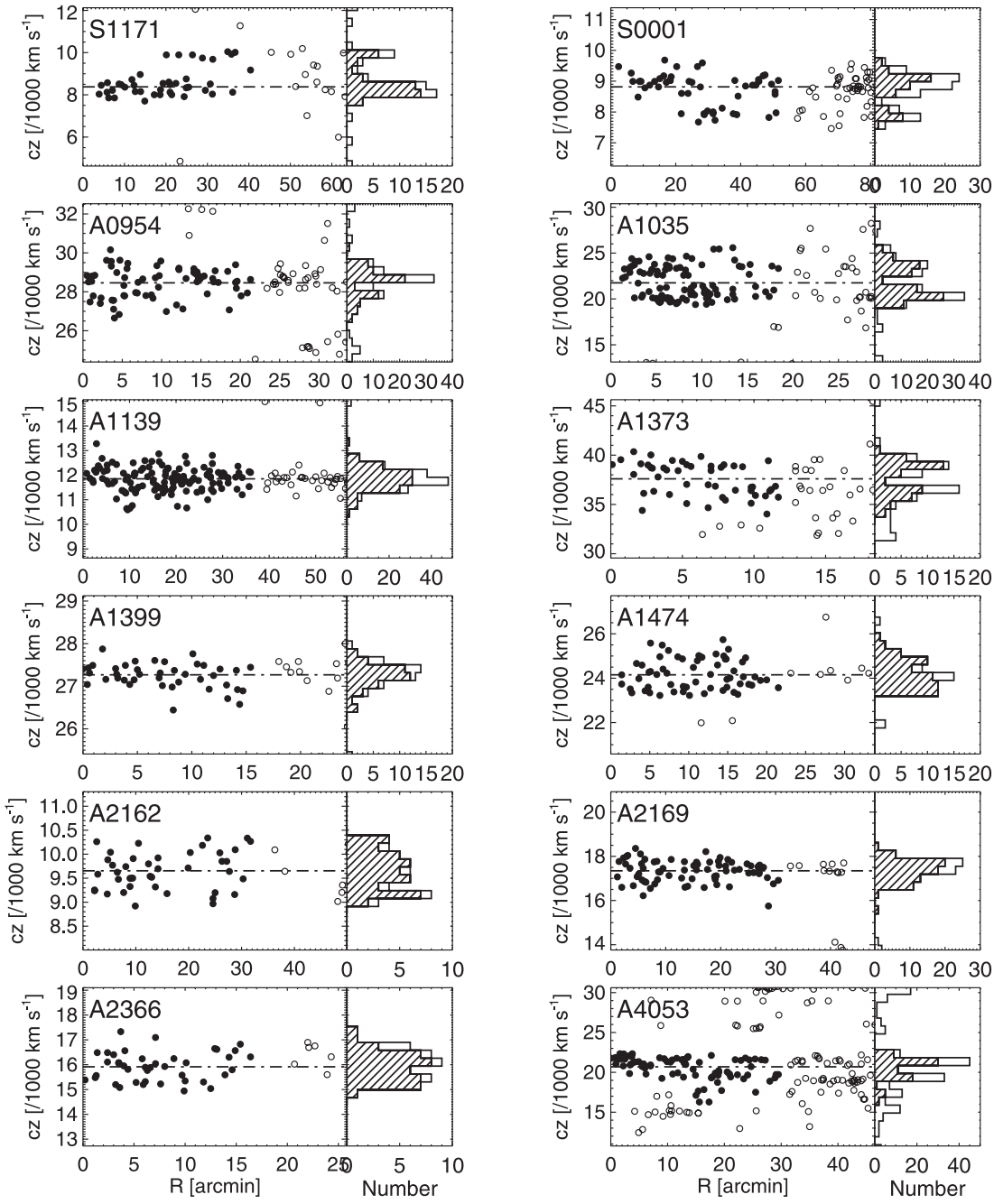

FIG. 2.—Radial velocity vs. clustercentric distance of galaxies and the velocity distribution for our 12 tentative rotating clusters. Filled circles indicate the galaxies selected as cluster members, while open circles are the galaxies not selected as cluster members. The horizontal dot-dashed lines indicate the systemic velocity of the clusters determined in Table 1. The velocity distributions for the member galaxies are shown by hatched histograms, and those for the all of the observed galaxies by open histograms.

10 clusters have rotation amplitudes in the range 190 km s^{-1} < $v_{\rm rot}$ < 830 km s^{-1} and velocity gradients in the range 400 km s^{-1} Mpc^{-1} < dv/dR < 1080 km s^{-1} Mpc^{-1}.

Figure 2 shows plots of radial velocity versus clustercentric distance of galaxies and the velocity distributions for the 12 tentative rotating clusters. In Figure 3, we show the spatial distribution of cluster galaxies with measured velocity. For most of the clusters, the galaxies whose velocities are greater than the systemic velocity of the cluster (*open circles*) and the galaxies whose velocities are less than this (*filled circles*) are spatially well separated by the rotation axis (Y1 or Y2). Interestingly, the position angles of the rotation axes, Y1 (determined from eq. [1]) and Y2 (determined from eq. [2]), coincide well (the difference between Y1 and Y2 is less than 20°) for all but three clusters (S0001, A1399, and A2169).

We plot the radial velocities as a function of projected distance along the direction perpendicular to the position angle (Θ_0) of rotation axis Y1 in Figure 4. Velocity gradients along the X1 axis are marginally seen in some clusters (A1035, A1373, A1474, and A2162) but not clearly seen in the others.

4. GLOBAL CLUSTER PROPERTIES

4.1. *Cluster Morphology*

In order to identify the connection between cluster morphology and cluster dynamics, it is useful to determine the ellipticity

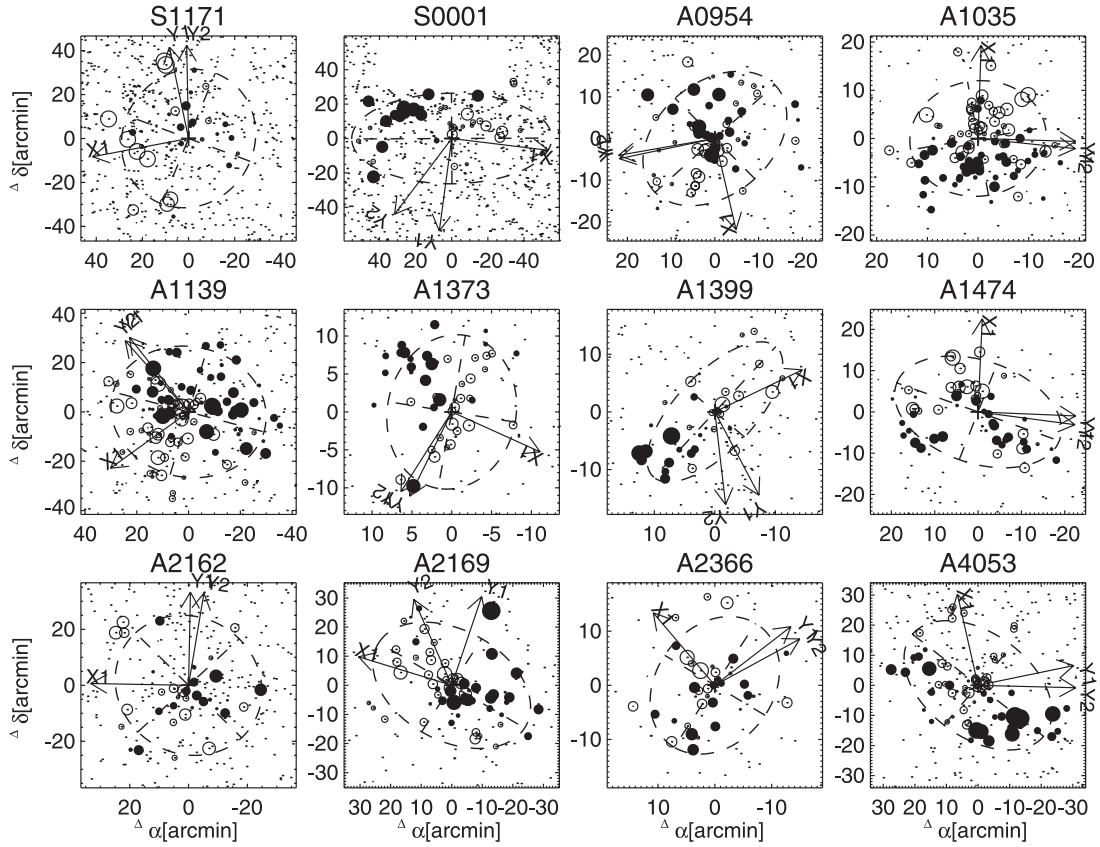

FIG. 3.—Spatial distribution of cluster galaxies with measured velocities in the 12 tentative rotating clusters. The cluster galaxies whose velocities are greater than the systemic velocity of their cluster are plotted with open circles, while those whose velocities are less than the systemic velocity are shown by filled symbols. The symbol size is proportional to the velocity deviation. The observed galaxies are represented by dots. The position angles, Θ_0 and Θ_1, derived using eqs. (1) and (2) are represented by arrows (axes Y1 and Y2). The axis perpendicular to the position angle of rotation axis Y1 is shown as X1. The dashed ellipses indicate the (twice enlarged) dispersion ellipse, and dashed lines denote the major and minor axis of the dispersion ellipse, respectively. [*See the electronic edition of the Journal for a color version of this figure.*]

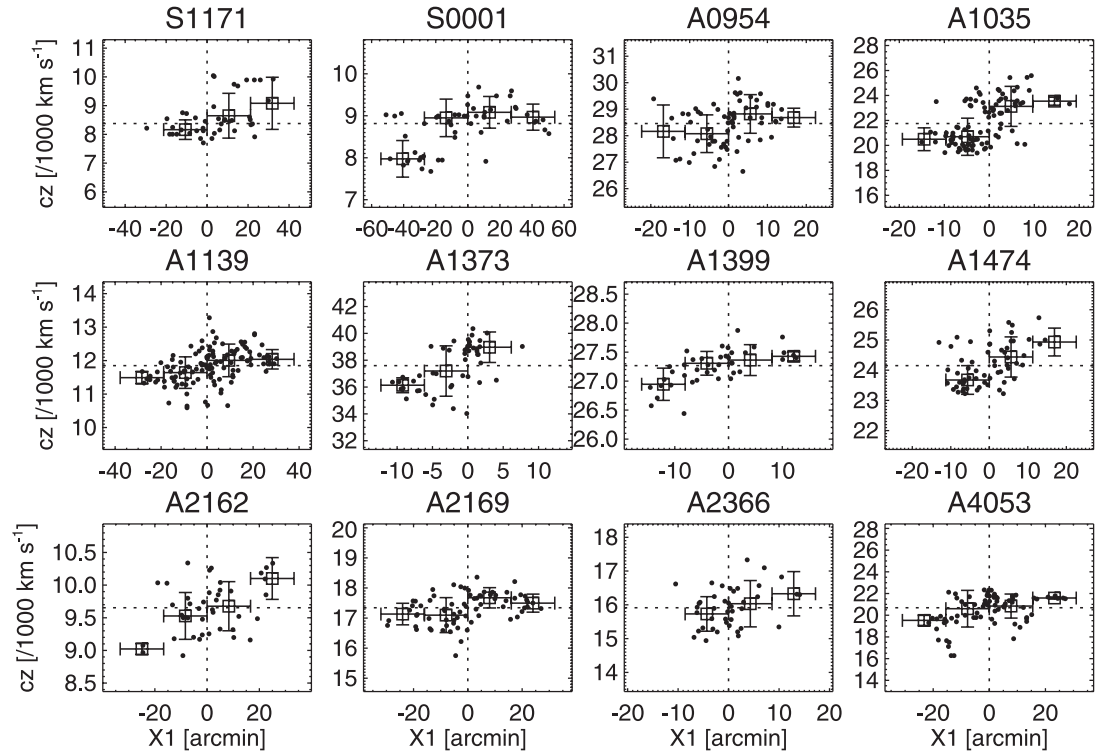

FIG. 4.—Radial velocities of cluster galaxies as a function of projected distance along axis X1 shown in Fig. 3. Open squares indicate the mean radial velocity of cluster galaxies in distance bins represented by the horizontal error bars. The vertical error bars denote the velocity dispersion of galaxies in each distance bin. [*See the electronic edition of the Journal for a color version of this figure.*]

TABLE 3
MORPHOLOGICAL PARAMETERS OF THE TENTATIVE ROTATING CLUSTERS

Cluster	Γ_A (kpc)	Γ_B (kpc)	Θ_2 (deg)	ϵ
S1171	537^{+47}_{-43}	482^{+38}_{-41}	159^{+25}_{-47}	$0.10^{+0.09}_{-0.09}$
S0001	978^{+72}_{-74}	465^{+66}_{-62}	90^{+5}_{-5}	$0.52^{+0.07}_{-0.07}$
A954.....	993^{+74}_{-71}	702^{+65}_{-67}	133^{+9}_{-11}	$0.29^{+0.08}_{-0.08}$
A1035.....	560^{+34}_{-32}	495^{+34}_{-34}	100^{+28}_{-20}	$0.12^{+0.08}_{-0.07}$
A1139.....	709^{+38}_{-36}	620^{+37}_{-38}	74^{+19}_{-16}	$0.13^{+0.07}_{-0.07}$
A1373.....	689^{+61}_{-56}	545^{+48}_{-45}	170^{+20}_{-15}	$0.21^{+0.09}_{-0.10}$
A1399.....	772^{+74}_{-74}	334^{+32}_{-32}	138^{+5}_{-5}	$0.57^{+0.06}_{-0.06}$
A1474.....	912^{+61}_{-62}	563^{+45}_{-43}	69^{+7}_{-6}	$0.38^{+0.07}_{-0.07}$
A2162.....	502^{+51}_{-47}	461^{+48}_{-50}	44^{+49}_{-42}	$0.08^{+0.11}_{-0.09}$
A2169.....	941^{+56}_{-57}	631^{+57}_{-56}	58^{+9}_{-8}	$0.33^{+0.07}_{-0.07}$
A2366.....	419^{+42}_{-39}	324^{+37}_{-36}	148^{+18}_{-22}	$0.23^{+0.09}_{-0.10}$
A4053.....	1061^{+70}_{-73}	676^{+56}_{-53}	51^{+6}_{-9}	$0.36^{+0.07}_{-0.07}$

and the orientation of a cluster using the spatial distribution of the selected member galaxies. To determine the cluster shape, we employ the dispersion ellipse of the bivariate normal frequency function of position vectors (see, e.g., Trumpler & Weaver 1953; Carter & Metcalfe 1980; Burgett et al. 2004). The dispersion ellipse is defined by Trumpler & Weaver (1953) as the contour at which the density is 0.61 times the maximum density of a set of points distributed normally with respect to two correlated variables, although the points need not be distributed normally in order to determine the proper cluster shape. From the first five moments of the spatial distribution,

$$\mu_{10} = \frac{1}{N}\sum_{i=1}^{N} X_i, \quad \mu_{01} = \frac{1}{N}\sum_{i=1}^{N} Y_i, \tag{3a}$$

$$\mu_{20} = \frac{1}{N}\sum_{i=1}^{N} X_i^2 - \left(\frac{1}{N}\sum_{i=1}^{N} X_i\right)^2, \tag{3b}$$

$$\mu_{11} = \frac{1}{N}\sum_{i=1}^{N} X_i Y_i - \frac{1}{N^2}\sum_{i=1}^{N} X_i \sum_{i=1}^{N} Y_i, \tag{3c}$$

$$\mu_{02} = \frac{1}{N}\sum_{i=1}^{N} Y_i^2 - \left(\frac{1}{N}\sum_{i=1}^{N} Y_i\right)^2, \tag{3d}$$

where X and Y are clustercentric distances in the direction of right ascension and declination, respectively, the semimajor and semiminor axes of the ellipse, Γ_A and Γ_B, are derived by solving the equation

$$\begin{vmatrix} \mu_{20} - \Gamma^2 & \mu_{11} \\ \mu_{11} & \mu_{02} - \Gamma^2 \end{vmatrix} = 0. \tag{4}$$

The position angle of the major axis, measured from north to east, is given by

$$\Theta_2 = \cot^{-1}\left(-\frac{\mu_{02} - \Gamma_A^2}{\mu_{11}}\right) + \frac{\pi}{2}, \tag{5}$$

and the ellipticity is defined by

$$\epsilon = 1 - \Gamma_B/\Gamma_A. \tag{6}$$

The major and minor axes, position angles, and ellipticities derived for our tentative rotating clusters are listed in Table 3. Interestingly, the ellipticities of S0001 ($\epsilon = 0.52$) and A1399 ($\epsilon = 0.57$) are unusually large compared with the other clusters. However, the ellipticity of S0001 might be uncertain, because no data are available beyond $\sim 30'$ north of the center of S0001, as seen in Figure 3.

4.2. *Analysis of Substructure*

The analysis of substructure is a useful diagnostic tool for understanding the dynamical state of galaxy clusters. A good discussion of several substructure tests is given by Pinkney et al. (1996). We have derived number density maps using the spatial position (two-dimensional; 2D) of member galaxies and performed one-dimensional (1D) and three-dimensional (3D) substructure tests for the sample of tentative rotating clusters.

The majority of 1D (velocity histogram) substructure tests are normality tests. We present the results of five 1D tests for tentative rotating clusters in Table 4. The values of the *I*-test (Teague et al. 1990) are shown in the second and the third columns; I_{90} is the critical value ("clRej") for rejecting the Gaussian hypothesis at 90% confidence. Therefore, a velocity distribution is considered to be non-Gaussian if $I > I_{90}$. We find that all clusters satisfy the Gaussian hypothesis using the *I*-test except S1171 and A4053.

The skewness, which is a measure of the degree of asymmetry of a distribution, and the confidence level at which it rejects normality are given in the fourth and fifth columns. Positive or negative skewness indicates that the distribution is skewed to the right or left, respectively, with a longer tail to that side the distribution

TABLE 4
PARAMETERS TESTING THE PRESENCE OF SUBSTRUCTURE

Cluster	I	I_{90}	Skewness	clRej	Kurtosis	clRej	AI	clRej	TI	clRej	Δ_{obs}	$f(\Delta_{sim} > \Delta_{obs})$
S1171	1.21	1.11	0.96	99.3	−0.45	10.0	0.58	73.0	1.57	98.3	68	0.335
S0001	0.93	1.09	−0.45	86.3	−0.92	89.9	−0.08	13.0	0.91	53.8	98	0.000
A954.....	0.97	1.07	−0.29	71.8	−0.64	68.4	−0.44	61.1	0.92	52.8	97	0.006
A1035.....	1.00	1.05	0.34	85.3	−1.24	100.0	1.07	96.4	0.74	99.9	167	0.000
A1139.....	1.02	1.04	−0.18	60.7	0.23	64.1	0.29	42.7	0.94	47.8	206	0.000
A1373.....	0.99	1.10	−0.27	61.9	−1.19	99.3	−0.82	88.9	0.82	87.8	90	0.000
A1399.....	1.07	1.11	−0.50	86.3	0.29	70.8	−0.62	76.2	0.90	52.5	75	0.001
A1474.....	0.95	1.08	0.41	83.3	−1.00	97.0	1.36	99.2	0.73	99.5	84	0.012
A2162.....	0.92	1.11	0.03	6.9	−1.11	95.9	−0.34	48.9	0.86	71.7	42	0.464
A2169.....	1.01	1.07	−0.45	91.1	0.07	48.8	−0.78	86.7	0.88	72.5	120	0.000
A2366.....	0.95	1.11	0.26	57.4	−0.73	56.8	0.63	77.0	0.78	93.9	41	0.707
A4053.....	1.20	1.07	−1.02	99.9	0.57	84.3	−1.59	99.8	0.87	78.6	174	0.000

maximum. The kurtosis, which is the degree to which a distribution is peaked, and the confidence level at which it rejects normality are given in the sixth and the seventh columns. Positive values indicate pointed or peaked distributions, while negative values indicate flattened or nonpeaked distributions. The skewness test rejects a Gaussian distribution with a confidence of over 99% only for S1171 and A4053, consistent with the result of the *I*-test. The kurtosis test rejects the hypothesis of Gaussianity for A1035, A1373, A1474, and A2162 with confidence of over 95%.

From the eighth to the eleventh column, we present the asymmetry index (AI) and the tail index (TI) introduced by Bird & Beers (1993) along with their confidence levels. The AI measures the symmetry in a population by comparing gaps in the data on the left and right sides of the sample median, and TI compares the spread of the data at the 90% level with the spread at the 75% level. The Gaussian hypothesis for A1035 and A1474 is rejected by both tests with a confidence level of over 95%.

We have constructed number density contours for the clusters using different bin sizes of $0.25R \times 0.25R$ Mpc^2 depending on the cluster size [$R = 4(\Gamma_A\Gamma_B)^{1/2}/1.5$]. Γ_A and Γ_B are in units of Mpc, 4 is an arbitrary constant, and 1.5 (Mpc) is a normalization constant. We have smoothed the contours using a cubic convolution interpolation method. The contour interval, (max density in cluster)/6, is also determined according to the maximum number density of the clusters. We plot the number density map in the first and third columns of Figure 5.

Using the velocity data and positional information for the galaxies, we have performed a Δ-test (Dressler & Shectman 1988), which computes local deviations from the systemic velocity ($v_{\rm sys}$) and dispersion (σ_p) of the entire cluster. For each galaxy, the deviation is defined by

$$\delta^2 = \frac{N_{nn}}{\sigma_p^2}[(v_{\rm local} - v_{\rm sys})^2 + (\sigma_{\rm local} - \sigma_p)^2], \qquad (7)$$

where N_{nn} is the number of galaxies that define the local environment, taken to be $\sim N_{\rm gal}^{1/2}$ in this study. The sum of δ over all galaxies in a cluster, Δ, is used to quantify the presence of substructure. It is approximately equal to the total number of galaxies in a cluster in the case of no substructure, while it is larger in the presence of substructure.

The statistical significance of the deviation is computed by Monte Carlo simulations. Velocities are randomly assigned to the galaxies at their observed positions, and $\Delta_{\rm sim}$ is computed for each simulated cluster. We construct 1000 simulated clusters and compute $\Delta_{\rm sim}$ for each simulation. We present $\Delta_{\rm obs}$, which is computed using real data, and the fraction of simulated clusters with $\Delta_{\rm sim} > \Delta_{\rm obs}$ in the final two columns of Table 4. Small values of $f(\Delta_{\rm sim} > \Delta_{\rm obs})$ indicate statistically significant substructure. Most clusters have small values of $f(\Delta_{\rm sim} > \Delta_{\rm obs})$, indicating significant substructures or spatially correlated velocities of galaxies, except for S1171, A2162, and A2366.

We plot the positions of cluster galaxies, represented by circles with radii proportional to e^{δ}, in the second and the fourth columns of Figure 5. A large circle denotes a galaxy that is deviant in either velocity or dispersion compared with nearby galaxies; therefore, groups of large circles indicate the presence of substructure. No substructures in S1171, A2162, and A2366 were found with the $f(\Delta_{\rm sim} > \Delta_{\rm obs})$ test, as confirmed in Figure 5.

5. DETAILED ANALYSIS OF INDIVIDUAL CLUSTERS

A single cluster in rotation is expected to show a spatial segregation of high- and low-velocity galaxies and to have a single number-density peak, unlike the case in which two clusters are still in the process of merging. Therefore, from our sample of tentative rotating clusters we select as probable rotating clusters those galaxy clusters that show a spatial segregation of high- and low-velocity galaxies in the spatial density map of Figure 3 and that also show a single peak in the number density map of Figure 5. We describe the selection of the individual probable rotating clusters in this section.

5.1. *Abell S1171*

Abell S1171 is the nearest ($z \sim 0.028$) cluster in the sample of tentative rotating clusters. In the plot of velocity versus clustercentric distance of the member galaxies (Fig. 2), it can be seen that some galaxies have large velocity deviations ($cz - \overline{cz} \sim 1400$ km s^{-1}) from the main body of the cluster ($\overline{cz} \sim 8400$ km s^{-1}). If we consider only galaxies in the cluster main body, rejecting these deviant galaxies ($cz > 9500$ km s^{-1}) as interlopers (in order to test the effect of this subcomponent), we obtain $|v_{\rm rot}|/\sigma_p = 0.33$ and $dv/dR = 299$ km s^{-1} Mpc^{-1}. Thus, this cluster is not included in the sample of tentative rotating clusters.

5.2. *Abell S0001*

Abell S0001 exhibits a low-velocity tail ($cz \sim 7800$ km s^{-1}) in the velocity histogram of Figure 2. The galaxies in this low-velocity tail are spatially concentrated, appearing as a substructure (to the northeast) in Figure 5. The number density map shows two local density maxima, which coincide with the positions of substructures. Therefore, the large amplitudes of the rotation and the velocity gradient are considered to be caused by two separate subclusterings. This cluster shows a large ellipticity, and the position angle of the rotation axis (Y1) shown in Figure 3 is similar to that of the cluster minor axis (Γ_B). However, the determination of the cluster's morphology is uncertain, since no data are available more than $\sim 30'$ from the north of the cluster center (see Fig. 3).

5.3. *Abell 954*

Abell 954 is included in both SDSS and 2dFGRS and is one of the most X-ray–luminous clusters in the sample of tentative rotating clusters. In Figure 3, the position angles of the rotation axes determined by the rotation fit (Y1) and the global velocity gradient fit (Y2) coincide well, but they appear not to be correlated with the position angle of the major or minor axis of the dispersion ellipse. The results of the 1D substructure tests in Table 4 show that the velocity distribution does not significantly deviate from Gaussian. The number density map and Dressler-Shectman (D-S) plot in Figure 5 show a weak sign of subclustering $\sim 14'$ to the southeast, and it is suspected that this subclustering might be the cause of the large rotation amplitude. In order to test the effect of the southeast subclustering, we fitted the velocities of member galaxies located within $10'$ of the cluster center using equations (1) and (2). The fitting resulted in $|v_{\rm rot}|/\sigma_p = 0.54$ and $dv/dR = 948$ km s^{-1} Mpc^{-1} with the same position angles of the rotation axes as the result based on all member galaxies. This implies that the rotation and the velocity gradient are generated in the core region with a single density peak. Therefore, we select this as a probable rotating cluster.

5.4. *Abell 1035*

Abell 1035 has the largest X-ray luminosity and velocity dispersion in the sample of tentative rotating clusters. While Flin & Krywult (2006) found no substructure using only positional information for its galaxies by applying a wavelet analysis,

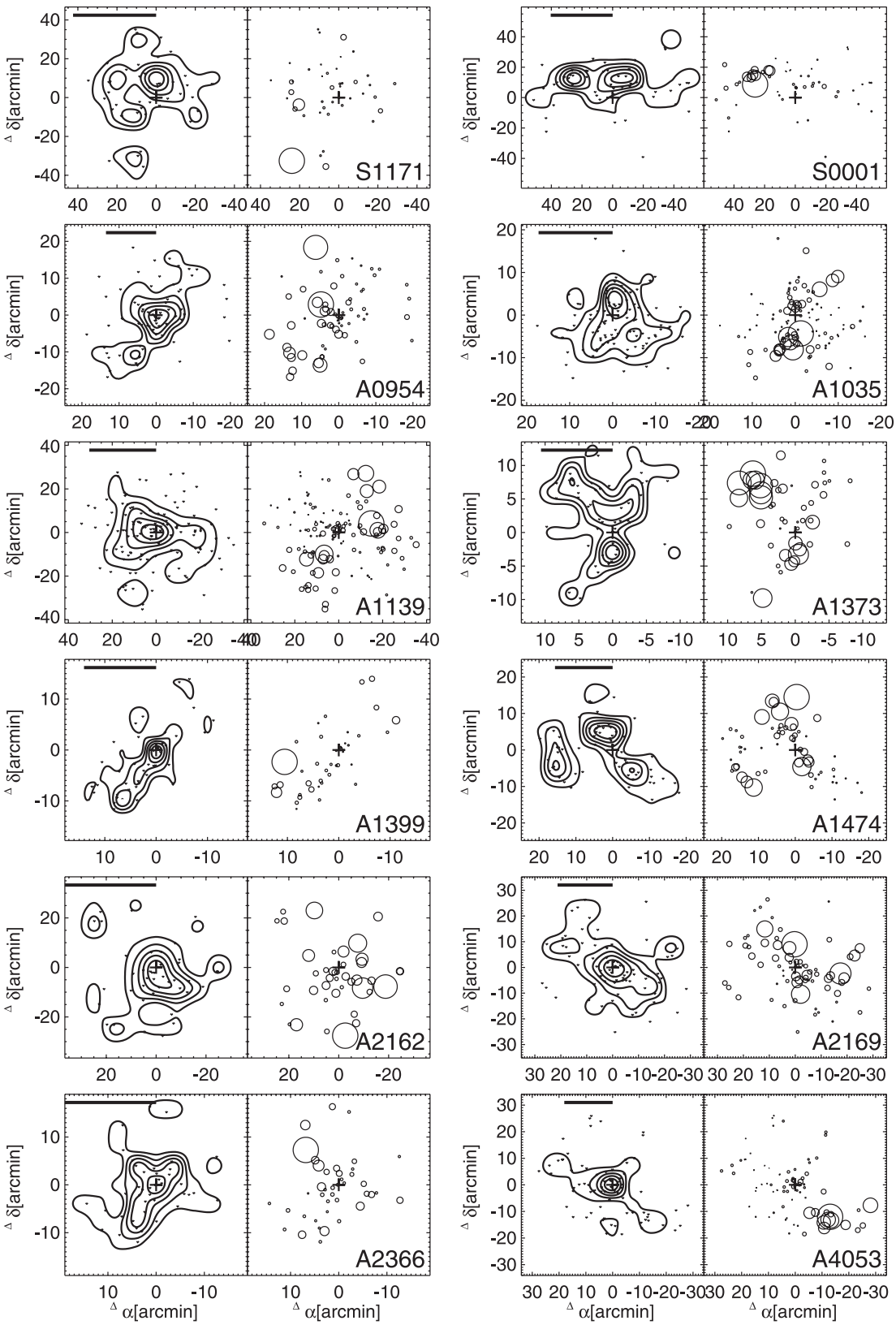

FIG. 5.—*Left columns*: Galaxy number density maps for tentative rotating clusters. The member galaxies are represented by dots, and number density contours are overlaid. The plus signs indicate the cluster centroids, and the thick horizontal bars represent a physical extent of 1 Mpc. *Right columns*: Dressler-Shectman plots for the same clusters. Each galaxy is plotted by a circle with diameter proportional to e^{δ}. North is up, and east is to the left.

Maurogordato et al. (1997) found a bimodal velocity distribution for this cluster using the velocity data for 19 member galaxies, as confirmed in Figure 2 based on the 97 member galaxies in this study. Our result in Figure 2 implies that substructures may exist. In Figure 3, the galaxies with velocities greater than the systemic velocity of the cluster (*open circles*) and those with velocities below the systemic velocity (*filled circles*) are clearly spatially separated by the rotation axes (Y1 and Y2). In addition, the D-S plot in Figure 5 shows two subclusterings (north and south) that coincide with high-density regions in the galaxy number density map. Therefore, the large amplitudes of the rotation and the velocity gradient, including the large velocity dispersion (listed in Table 1), can be explained as being due to two superposed or interacting clusters with slightly different systemic velocities.

Aryal & Saurer (2006) found that the spin-vector orientations of the galaxies in this cluster tend to lie parallel to the Local Supercluster (LSC) plane and that the spin-vector projections of the galaxies tend to be oriented perpendicular with respect to the direction of the LSC center. In this study, we find that the angle between the rotation axis (Y1) of this cluster and the LSC plane is 56^{+11}_{-9} deg. Since the angle between the spin-vector orientations of the galaxies in this cluster and the LSC plane was found to be less than 45° by Aryal & Saurer (2006), it appears that the spin-vector orientations determined by Aryal & Saurer are not related to the rotation axis of this cluster as determined in this study.

5.5. *Abell 1139*

Abell 1139 is included in both SDSS and 2dFGRS and has the largest number of member galaxies in our sample. A global velocity gradient for this cluster was identified by Burgett et al. (2004) using 2dFGRS data for 106 member galaxies. We confirm this global velocity gradient or rotation using 122 member galaxies with the aid of SDSS data (see Fig. 4). The D-S plot in Figure 5 shows the presence of strong substructures to the northwest and to the southeast, while the velocity histogram shows a unimodal distribution. It is known that the galaxy positional information alone shows no clear substructure for this cluster (e.g., Krywult et al. 1999; Flin & Krywult 2006), but distinguishable substructure is found based on combined positional information and velocity data (e.g., Burgett et al. 2004). As can be seen in the spatial velocity plot in Figure 3, the substructures are due to galaxies with different radial velocities. Interestingly, unlike Abell 1035, the galaxy number density map shows a single density peak near the cluster center rather than strong concentrations around two substructures. This may indicate a single cluster in rotation or two overlapping clusters that are either merging or departing from each other, as pointed out by Burgett et al. (2004). Therefore, we select this cluster as a probable rotating cluster.

5.6. *Abell 1373*

Abell 1373 is the most distant cluster ($z \sim 0.125$) in our sample of tentative rotating clusters, and it was surveyed in both SDSS and 2dFGRS. The velocity distribution is bimodal, and the galaxies with high velocities ($cz \sim 39{,}000$ km s^{-1}) and those with low velocities ($cz \sim 36{,}000$ km s^{-1}) are spatially separated by the rotation axis (see Fig. 3). Similar to the case of Abell 1035, the substructures introduced by the clustering of galaxies with different velocities coincide with the galaxy number density peaks, implying that the large amplitudes of the rotation and the velocity gradient are induced by two disparate groups (see Fig. 5).

5.7. *Abell 1399*

Abell 1399 is one of the member clusters in the Leo A supercluster (Einasto et al. 2001). This cluster has the smallest velocity dispersion in our sample of tentative rotating clusters, and it was surveyed in both SDSS and 2dFGRS. The velocity distribution is unimodal, but the spatial velocity plot of Figure 3 shows a segregation of galaxies with different velocities. Intriguingly, the dispersion ellipse is significantly flatted, with an ellipticity of 0.57. Since the position angles of the dispersion ellipse (138° for the major axis and 48° for the minor axis) deviate from those of the rotation axes (207° for Y1 and 186° for Y2), it appears that the high ellipticity is not related to a global rotation of this cluster. Figure 5 shows that there is no strong sign of a correlation between the number density peaks and the substructures. Therefore, we select this cluster as a probable rotating cluster.

5.8. *Abell 1474*

Abell 1474 is one of the member clusters in the Virgo-Coma supercluster (Einasto et al. 2001). Flin & Krywult (2006) found no substructure using only positional information for the galaxies, but the 1D substructure tests indicate that the velocity distribution deviates significantly from Gaussian. In Figure 5, the D-S plot shows that there are three substructures (to the northeast, the southwest, and the southeast) that coincide with the three number density peaks in the left panel. This indicates that the large amplitudes of the rotation and the velocity gradient are due to the different velocities of subgroups.

5.9. *Abell 2162*

Abell 2162 is one of the nearest clusters in our sample and is a member of the Hercules supercluster (Einasto et al. 2001). Neither a distinct substructure nor a significant local density peak is found aside from the cluster center in Figure 5. Interestingly, it appears that the radial distribution of the member galaxies in Figure 2 exhibits a discontinuity at $\sim 18'$. If we therefore compute the rotation amplitude and the global velocity gradient using only the galaxies in the inner region ($<18'$), we obtain $|v_{\rm rot}|/\sigma_p = 0.64$ and $dv/dR = 635$ km s^{-1} Mpc^{-1}, still satisfying our criteria for a rotating cluster. Therefore, we select this as a probable rotating cluster.

5.10. *Abell 2169*

In Figure 3, the galaxies that have velocities greater than the systemic velocity of Abell 2169 (*open circles*) and those whose velocities are less than the systemic velocity (*filled circles*) are well separated by the rotation axis (Y1). The position angle (342°) of the rotation axis (Y1) is similar to that (328°) of the minor axis of the dispersion ellipse, implying that the flatness may be caused by cluster rotation. The substructures (northeast and southwest) seen in the D-S plot are separated by the cluster centroid, which coincides with the single peak in number density. Therefore, this cluster is selected as a probable rotating cluster.

5.11. *Abell 2366*

Jones & Forman (1999) classified the morphology of Abell 2366 using *Einstein* X-ray images as a "single," meaning a cluster in which no substructure or departure from symmetry is found. Flin & Krywult (2006) also found no substructure by using only positional information for the galaxies and applying a wavelet analysis. Similarly, the galaxy number density map and the D-S plot in Figure 5 indicate no strong evidence of substructure. Therefore, we select this cluster as a probable rotating cluster.

5.12. *Abell 4053*

Abell 4053 is one of the member clusters in the Pisces-Cetus supercluster (Porter & Raychaudhury 2005), and it is known to be contaminated by a foreground group at $z = 0.0501$ (Mazure et al.

TABLE 5

SUMMARY OF GLOBAL KINEMATIC PROPERTIES FOR TENTATIVE ROTATING CLUSTERS

CLUSTER	SUBSTRUCTURE? 1D	2D	3D	MORPHOLOGY	DYNAMICAL EQUILIBRIUM?	PROBABLE ROTATING CLUSTER?
S1171	Yes	Yes	No	Spherical	...	No
S0001	No	Yes	Yes	Elongated?	...	No
A954.....	No	Yes	Yes	Elongated	Yes	Yes
A1035.....	Yes	Yes	Yes	Spherical	...	No
A1139.....	No	No	Yes	Spherical	Yes	Yes
A1373.....	Yes	Yes	Yes	Elongated	...	No
A1399.....	No	No	Yes	Elongated	Yes	Yes
A1474.....	Yes	Yes	Yes	Elongated	...	No
A2162.....	Yes	No	No	Spherical	Yes	Yes
A2169.....	No	No	Yes	Elongated	Yes	Yes
A2366.....	No	No	No	Elongated	Yes	Yes
A4053.....	Yes	No	Yes	Elongated	...	No

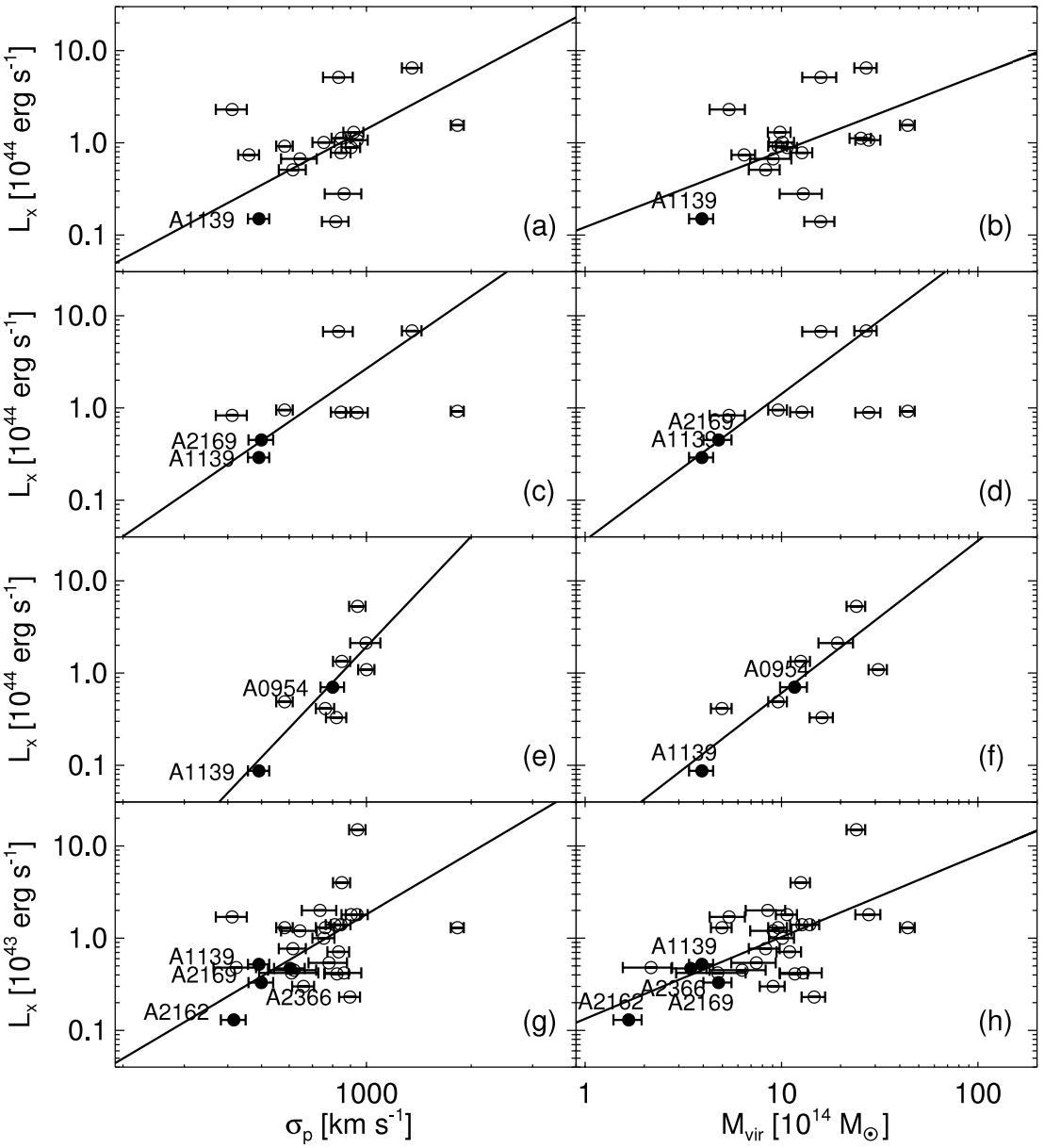

FIG. 6.—X-ray luminosity L_X (0.1–2.4 keV) vs. velocity dispersion and virial mass for the probable rotating clusters (*filled circles*) compared with the nonrotating galaxy clusters (*open circles*) for the 56 selected galaxy clusters. X-ray luminosities in (*a*) and (*b*) are from Böhringer et al. (2000), those in (*c*) and (*d*) from Ebeling et al. (1998, 2000), those in (*e*) and (*f*) from Böhringer et al. (2004), and those (0.5–2.0 keV) in (*g*) and (*h*) from Ledlow et al. (2003). The solid lines indicate the best fit for each panel.

TABLE 6
VELOCITY DISPERSIONS AND VIRIAL MASSES FOR PROBABLE ROTATING CLUSTERS

Cluster	σ_p (km s^{-1})	$\sigma_{p,r}$ (km s^{-1})	$M_{\rm vir}$ ($10^{14}\ M_\odot$)	$M_{{\rm vir},r}$ ($10^{14}\ M_\odot$)
A954.....	801^{+63}_{-62}	719^{+74}_{-67}	$11.65^{+1.92}_{-1.73}$	$9.39^{+2.03}_{-1.67}$
A1139.....	491^{+39}_{-32}	423^{+40}_{-36}	$3.93^{+0.66}_{-0.49}$	$2.92^{+0.58}_{-0.48}$
A1399.....	289^{+43}_{-39}	248^{+44}_{-38}	$1.06^{+0.34}_{-0.27}$	$0.77^{+0.30}_{-0.22}$
A2162.....	416^{+32}_{-31}	377^{+40}_{-39}	$1.67^{+0.26}_{-0.24}$	$1.37^{+0.31}_{-0.27}$
A2169.....	499^{+42}_{-40}	431^{+45}_{-43}	$4.78^{+0.83}_{-0.74}$	$3.56^{+0.78}_{-0.67}$
A2366.....	604^{+58}_{-53}	569^{+65}_{-62}	$3.45^{+0.69}_{-0.58}$	$3.06^{+0.73}_{-0.63}$

1996). The galaxies in the foreground group ($cz \sim 15{,}000$ km s^{-1}) are evident in Figure 2 and were rejected when we determined the membership of Abell 4053. However, the galaxies in the low-velocity tail ($cz \sim 17{,}500$ km s^{-1}) were selected as members of Abell 4053. These galaxies are found in the region to the southwest of the cluster centroid (see Fig. 3) and are detected as a subcluster in the D-S plot. In order to estimate the effect of these galaxies in the low-velocity tail, we determine the amplitudes of the rotation and the velocity gradient using only the galaxies in the main body ($cz > 18{,}000$ km s^{-1}). The fitting results in $|v_{\rm rot}|/\sigma_p = 0.47$ and $dv/dR = 716$ km s^{-1} Mpc^{-1}, which does not satisfy the criteria for a tentative rotating cluster. Therefore, this cluster is not selected as a probable rotating cluster.

We summarize the global kinematic properties for the 12 tentative rotating clusters in Table 5. The first column gives the Abell identification. The second through fourth columns list the existence of substructure as indicated by the 1D, 2D, and 3D tests, respectively. The cluster morphology determined in § 4.1 is given in the fifth column: "spherical" for ellipticity less than 0.2 and "elongated" for ellipticity $\geq$0.2. The dynamical status determined in § 6 is given in the sixth column, and the selection of probable rotating clusters is in the final column.

6. DISCUSSION

6.1. *Dynamical Status of Probable Rotating Clusters*

A study of the dynamical state of the probable rotating clusters is useful for understanding the origin of the global rotation across each cluster. It is expected from self-similar models that a relationship $L_{\rm X} \propto \sigma_p^4$ between the X-ray luminosity and the velocity dispersion of the clusters will exist (e.g., Quintana & Melnick 1982). For galaxy clusters in SDSS, Popesso et al. (2005) found $L_{\rm X} \propto \sigma_p^{3.68\pm0.25}$. For galaxy clusters in 2dFGRS, Hilton et al. (2005) found a relation $L_{\rm X} \propto \sigma_p^{4.8\pm0.7}$ and suggested that high-$L_{\rm X}$ clusters are more dynamically evolved systems than the low-$L_{\rm X}$ clusters. In Figure 6, we plot the X-ray luminosity as a function of velocity dispersion and virial mass for the probable rotating clusters (*filled circles*) for which X-ray luminosities are available in the literature, compared with the nonrotating galaxy clusters (*open circles*) that have X-ray luminosities in the literature, out of the 56 selected galaxy clusters. We plot the X-ray luminosities from different literature sources separately. It appears that most galaxy clusters shown in Figure 6 follow the $L_{\rm X}$-σ_p and $L_{\rm X}$-$M_{\rm vir}$ relations (*solid lines*) determined in this study. Moreover, several interesting features are seen in the probable rotating clusters. First, they do not deviate from the best-fit line, implying that these clusters are in dynamical equilibrium. Secondly, the velocity dispersions and the virial masses for the probable rotating clusters appear to be smaller than those for the nonrotating clusters. In addition, the X-ray luminosities for the probable rotating clusters also appear to be smaller than those of the nonrotating clusters. If we adopt the result of Hilton et al. (2005), the probable rotating clusters that have low X-ray luminosities might have a lower fraction of early-type, passively evolving galaxies than the galaxy clusters with high X-ray luminosities.

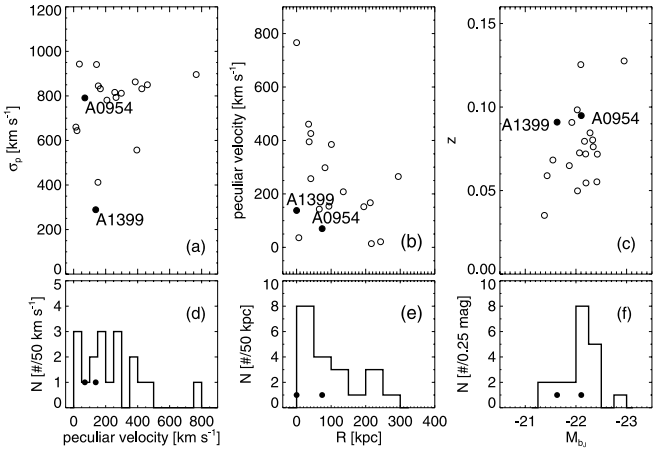

FIG. 7.—(*a*) Velocity dispersion as a function of the absolute value of the peculiar velocities of BCGs, (*b*) redshift as a function of the absolute magnitudes of the BCGs in the $b_{\rm J}$ band, and (*c*) absolute value of peculiar velocity as a function of the clustercentric distances of the BCGs for two probable rotating clusters (*filled circles*) compared with 20 nonrotating galaxy clusters (*open circles*) among the 56 selected galaxy clusters. Histograms of (*d*) the peculiar velocities, (*e*) the clustercentric distances, and (*f*) the absolute magnitudes in the $b_{\rm J}$ band of the BCGs are also shown for the 22 galaxy clusters, including the two probable rotating clusters. The two probable rotating clusters are marked by filled circles in (*d*), (*e*), and (*f*).

If galaxy clusters rotate, the velocity dispersions and the corresponding virial masses should be corrected for the cluster rotation (see, e.g., Kalinkov et al. 2005). We derived the velocity dispersions around the best-fit rotation curve of equation (1) and the corresponding corrected virial masses for the probable rotating clusters. The results are summarized in Table 6. The second and third columns represent, respectively, the velocity dispersion about the mean velocity of the cluster and that about the best-fit rotation curve of equation (1). The fourth and fifth columns represent, respectively, the virial mass using the uncorrected (second column) velocity dispersion and that using the rotation-corrected (third column) velocity dispersion. The individual velocity dispersions are reduced by 6%–14% and on average are reduced by 11%. The corresponding virial masses are also reduced by 11%–27%, on average by 21%.

The dynamics of the brightest cluster galaxies (BCGs) or cD galaxies in galaxy clusters are also useful for understanding the formation history of galaxy clusters (see, e.g., Oegerle & Hill 2001). In particular, the peculiar velocity of the BCG, defined by $v_p = v_{\rm BCG} - v_{\rm cl}$, where $v_{\rm BCG}$ is the BCG's radial velocity and $v_{\rm cl}$ is the mean velocity of the cluster, is a useful indicator of the dynamical state of a cluster (Oegerle & Hill 2001). To estimate the peculiar velocities of BCGs in clusters, we first identified the BCGs that have the smallest $b_{\rm J}$ magnitudes in the catalog of member galaxies for the 56 selected galaxy clusters. Then we conducted a visual inspection of cluster images to determine whether there are any galaxies brighter than the selected BCGs, using the catalog of member galaxies. Since some very bright galaxies in the clusters were not covered as a result of observational difficulties, such as fiber collision and saturation, we finally selected 20 galaxy clusters for which the BCGs in the catalog agree with those in the images. Using this sample of 20 clusters, we plot in Figure 7 the absolute value of the peculiar velocity of the BCGs as a function of clustercentric distance, the redshift of the clusters

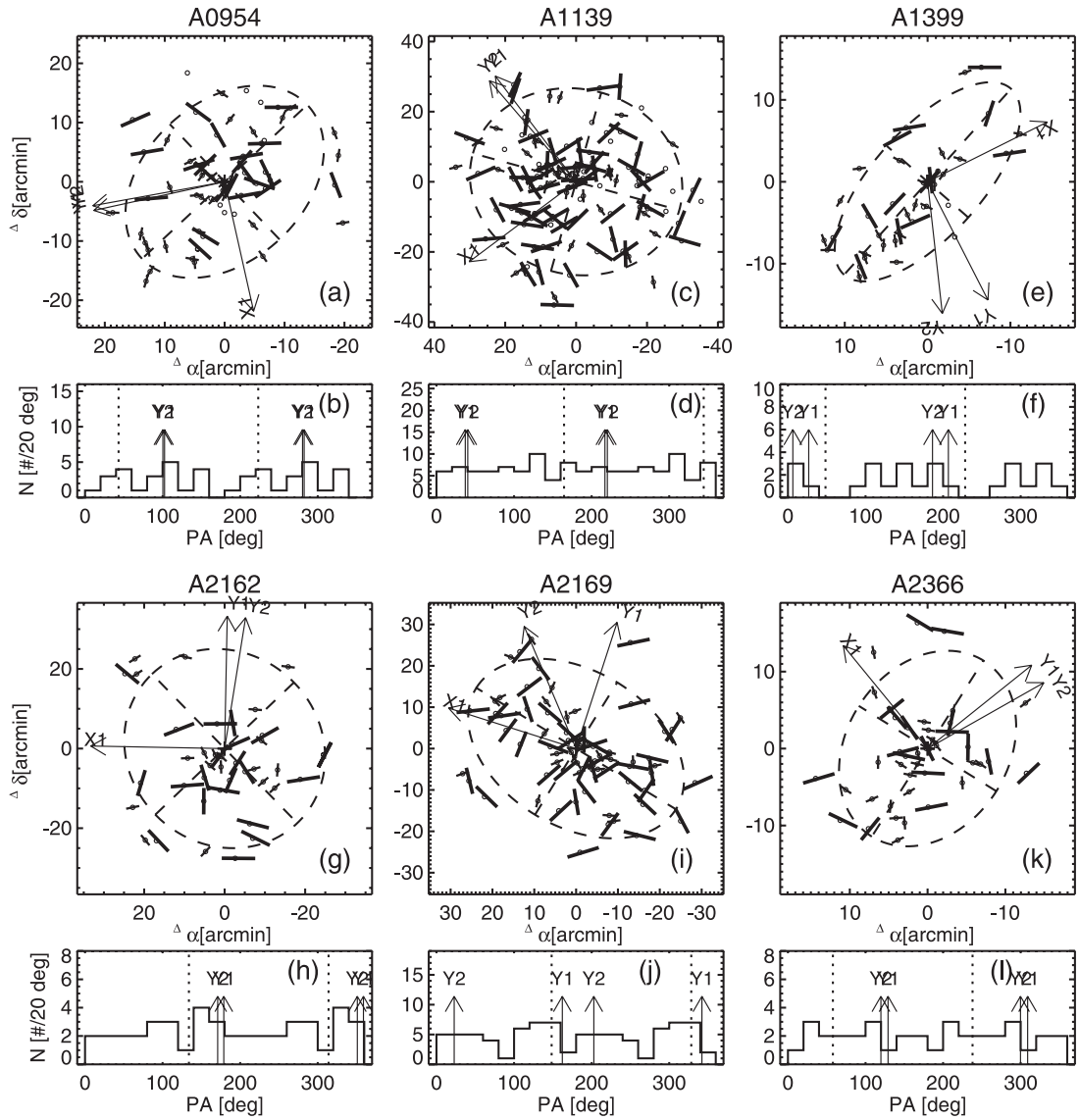

FIG. 8.—*Upper panels*: Spatial distribution of the projected spin-vector orientations of cluster galaxies in six probable rotating clusters. The cluster galaxies are plotted as open circles. Long solid bars represent the projected spin-vector orientations for the moderately edge-on galaxies (axial ratio less than 0.72 in SDSS and eccentricity equal to or greater than 0.33 in 2dFGRS), while short solid bars represent those for the face-on galaxies (axial ratio equal to or greater than 0.72 in SDSS and eccentricity less than 0.33 in 2dFGRS). The galaxies with unknown orientations are plotted as lone open circles. The dispersion ellipse and the rotation axes (Y1 and Y2) shown in Fig. 3 are overlaid. *Lower panels*: Histograms for the projected spin-vector orientations of cluster galaxies. We present histograms for only the moderately edge-on galaxies. The rotation axes (Y1 and Y2) are shown by vertical arrows and the minor axis of the dispersion ellipse is represented by vertical dotted lines. [*See the electronic edition of the Journal for a color version of this figure.*]

as a function of the BCG absolute magnitude in the b_J band, and the cluster velocity dispersion as a function of the absolute value of the peculiar velocity of the BCGs. It can be seen that the absolute values of the peculiar velocities of the BCGs are in the range 10–780 km s^{-1} and that the median value of the peculiar velocities is 257 km s^{-1}. The mean uncertainty in the values of the peculiar velocities is 168 km s^{-1}. In addition, the clustercentric distances of the BCGs are in the range 0–300 kpc, and the median value of the clustercentric distances is 82 kpc. Interestingly, the BCG peculiar velocities and clustercentric distances for two (Abell 954 and Abell 1399) of the probable rotating clusters are smaller than the median value of each parameter. These small values indicate that the clusters are in dynamical equilibrium. This may imply that the clusters have not undergone a recent merger if the clusters were formed through repeated merging. In addition, the absolute magnitudes of BCGs for these two probable rotating clusters do not show any significant deviation from the distribution for the nonrotating galaxy clusters.

6.2. *Probable Rotating Clusters and Spatial Orientation of Cluster Galaxies*

An interesting connection between the global rotation of clusters and the anisotropy in galaxy alignments for such clusters is expected in the context of the angular momentum of galaxy clusters:

1. Aryal & Saurer (2004, 2005, 2006) found that the anisotropy in galaxy alignments increases systematically from early-type (B-M type I) to late-type (B-M types II–III and III) clusters. Interestingly, four (A1139, A1399, A2162, and A2169) of six probably rotating clusters in this study are late-type clusters. Therefore, there may exist a connection between the rotation axes of

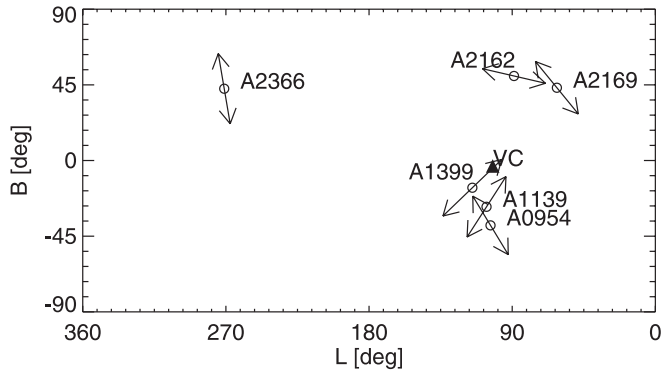

FIG. 9.—All-sky plot of six probable rotating clusters along with their rotation axes (Y1). *L* and *B* represent supergalactic longitude and latitude, respectively. Arrows represent the rotation axis of each cluster, and their length denotes the relative rotation amplitude, $|v_{\rm rot}|/\sigma_p$. The Virgo Cluster is shown as a triangle. The LSC plane goes through the X-axis.

the probable rotating clusters in this study and the spin-vector orientations of cluster galaxies. In order to examine this connection, we present in Figure 8 the spatial distribution and a histogram of the projected spin-vector orientations of the galaxies in these six probable rotating clusters. We used the 2dFRGS orientation parameter (ORIENT) and the SDSS *g*-band isophotal position angle parameter (isoPhi_g) as the projected spin-vector orientations for cluster galaxies (Colless et al. 2001; Stoughton et al. 2002). The position angles of the projected orientations for the cluster galaxies are measured in the range 0°–180° but are plotted twice over 0°–360°. Figure 8 shows that there is no strong anisotropy in the spin-vector orientations of cluster galaxies (i.e., no strong peaks in the histograms). Therefore, it is difficult to compare the position angles of the rotation axes with the spin-vector orientations of the cluster galaxies.

2. It was found that the spin-vector orientations of galaxies in clusters tend to lie parallel to the LSC plane (Aryal & Saurer 2006; Hu et al. 2006). In order to investigate the connection between the rotation axes of rotating clusters and the LSC plane, we plot in Figure 9 the all-sky distribution of six probable rotating clusters with their rotation axes (Y1) in supergalactic coordinates. It appears that there is no preferred direction of rotation axis for these clusters, whereas the spin-vector orientations of cluster galaxies from Aryal & Saurer (2006) and Hu et al. (2006) tend to lie parallel to the LSC plane (this result does not change if we use Y2 instead of Y1).

Since we do not have three-dimensional information about the rotation axes for rotating clusters and the three-dimensional spin-vector orientations of cluster galaxies in this study, it is difficult to make conclusions about the connection between the global rotation of clusters and the anisotropy in galaxy alignments for clusters at this point. Therefore, it is necessary to study the three-dimensional spatial orientations of galaxies for these rotating clusters to investigate any such connection.

6.3. *Cosmological Implications of Probable Rotating Clusters*

In a study based on the model proposed by Li (1998), in which the global rotation of the universe may provide angular momentum to celestial bodies upon their formation, Godłowski et al. (2005) found vanishing angular momenta for the masses corresponding to galaxy groups using Tully's galaxy groups. They suggested the existence of nonvanishing angular momenta for smaller and larger structures (compact galaxy groups and rich galaxy clusters). However, the nonvanishing angular momenta for galaxy clusters were found indirectly, based on a study of the galaxy orientations. In this study, we found nonvanishing angular momenta for galaxy clusters directly, based on a dynamical analysis. This result is consistent with that of Godłowski et al. (2005). However, we found that the estimated masses for rotating clusters are in the range 10^{14}–$10^{15}\ M_\odot$ (see Table 6). In addition, we could not identify rotating clusters more massive than $2 \times 10^{15}\ M_\odot$. Intriguingly, the mass range of rotating clusters in this study corresponds to the mass scale (10^{14}–$10^{15}\ M_\odot$) with *vanishing* angular momentum predicted by Godłowski et al. (2003). Since the masses of Tully's galaxy groups used by Godłowski et al. (2005) are expected to be smaller than those of the Abell clusters used in this study, this contradiction in the mass scale between theory and observations should be investigated further.

7. SUMMARY

We have presented the results of a search for galaxy clusters that show an indication of global rotation, using a spectroscopic sample of galaxies in SDSS and 2dFGRS. Our results are summarized as follows:

1. We have determined the member galaxies of 899 Abell clusters covered in SDSS and 2dFGRS. We have estimated the ratio of rotation amplitude to velocity dispersion and the velocity gradient for 56 clusters in which the number of member galaxies is greater than or equal to 40.
2. Among these 56 clusters, we have selected 12 tentative rotating clusters that have large values of the ratio of rotation amplitude to velocity dispersion (>0.53) and of the velocity gradient (>380 km s^{-1} Mpc^{-1}).
3. We have determined the cluster morphology for the 12 tentative rotating clusters using the dispersion-ellipse method. The ellipticity of the dispersion ellipse is in the range 0.08–0.57, and the position angle of its major and minor axes appears not to be related to the position angles of the rotation axes (Y1 and Y2).
4. We have investigated the presence of substructure (1D, 2D, and 3D) for the sample of tentative rotating clusters. Dressler-Shectman plots show that the majority (nine out of 12) show evidence of substructure due to spatially correlated velocities of the member galaxies.
5. We have selected six probable rotating clusters (Abell 954, 1139, 1399, 2162, 2169, and 2366) that show a single number-density peak around the cluster center with a spatial segregation of the high- and low-velocity member galaxies.
6. The probable rotating clusters do not deviate significantly from the relation between X-ray luminosity and the velocity dispersion or the virial mass of the cluster. The peculiar velocities and the clustercentric distances of BCGs for two of the probable rotating clusters (Abell 954 and Abell 1399) indicate that they may be in dynamical equilibrium and have undergone no recent merging.

It will be interesting to investigate the dynamical state of the probable rotating clusters using X-ray data in order to compare the properties of the intracluster medium and those of their member galaxies.

We would like to thank the referee, B. Aryal, for useful comments. We also would like to thank all the people involved in creating the SDSS, 2dFGRS, and NED. Funding for the SDSS and SDSS-II has been provided by the Alfred P. Sloan Foundation, the Participating Institutions, the National Science Foundation, the US Department of Energy, the National Aeronautics

and Space Administration, the Japanese Monbukagakusho, the Max Planck Society, and the Higher Education Funding Council for England. The SDSS Web Site is http://www.sdss.org. The SDSS is managed by the Astrophysical Research Consortium for the Participating Institutions. The Participating Institutions are the American Museum of Natural History, Astrophysical Institute Potsdam, the University of Basel, the University of Cambridge, Case Western Reserve University, the University of Chicago, Drexel University, Fermilab, the Institute for Advanced Study, the Japan Participation Group, Johns Hopkins University, the Joint Institute for Nuclear Astrophysics, the Kavli Institute for Particle Astrophysics and Cosmology, the Korean Scientist Group, the Chinese Academy of Sciences (LAMOST), Los Alamos National Laboratory, the Max Planck Institute for Astronomy, the Max Planck Institute for Astrophysics, New Mexico State University, Ohio State University, the University of Pittsburgh, the University of Portsmouth, Princeton University, the US Naval Observatory, and the University of Washington. This research has made use of the NASA/IPAC Extragalactic Database (NED), which is operated by the Jet Propulsion Laboratory, California Institute of Technology, under contract with the National Aeronautics and Space Administration. This work was supported in part by grant R01-2004-000-10490-0 from the Basic Research Program of the Korea Science and Engineering Foundation.

REFERENCES

Abell, G. O., Corwin, H. G., Jr., & Olowin, R. P. 1989, ApJS, 70, 1
Aryal, B., & Saurer, W. 2004, A&A, 425, 871
———. 2005, A&A, 432, 841
———. 2006, MNRAS, 366, 438
Beers, T. C., Flynn, K., & Gebhardt, K. 1990, AJ, 100, 32
Bird, C. M., & Beers, T. C. 1993, AJ, 105, 1596
Biviano, A., Durret, F., Gerbal, D., Le Fèvre, O., Lobo, C., Mazure, A., & Slezak, E. 1996, A&A, 311, 95
Böhringer H., et al. 2000, ApJS, 129, 435
———. 2004, A&A, 425, 367
Burgett, W. S., et al. 2004, MNRAS, 352, 605
Carter, D., & Metcalfe, N. 1980, MNRAS, 191, 325
Colless, M., et al. 2001, MNRAS, 328, 1039
den Hartog, R., & Katgert, P. 1996, MNRAS, 279, 349
Dressler, A., & Shectman, S. A. 1988, AJ, 95, 985
Dupke, R. A., & Bregman, J. N. 2001a, ApJ, 547, 705
———. 2001b, ApJ, 562, 266
———. 2005, ApJS, 161, 224
———. 2006, ApJ, 639, 781
Ebeling, H., Edge, A. C., Allen, S. W., Crawford, C. S., Fabian, A. C., & Huchra, J. P. 2000, MNRAS, 318, 333
Ebeling, H., Edge, A. C., Böhringer, H., Allen, S. W., Crawford, C. S., Fabian, A. C., Voges, W., & Huchra, J. P. 1998, MNRAS, 301, 881
Einasto, M., Einasto, J., Tago, E., Müller, V., & Andernach, H. 2001, AJ, 122, 2222
Fadda, D., Girardi, M., Giuricin, G., Mardirossian, F., & Mezzetti, M. 1996, ApJ, 473, 670
Flin, P., & Krywult, J. 2006, A&A, 450, 9
Godłowski, W., Szydłowski, M., & Flin, P. 2005, Gen. Relativ. Gravitation, 37, 615
Godłowski, W., Szydłowski, M., Flin, P., & Biernacka, M. 2003, Gen. Relativ. Gravitation, 35, 907
Hilton, M., et al. 2005, MNRAS, 363, 661
Hu, F.-X., Wu, G.-X., Song, G.-X., Yuan, Q.-R., & Okamura, S. 2006, Ap&SS, 302, 43
Jones, C., & Forman, W. 1999, ApJ, 511, 65
Kalinkov, M., Valchanov, T., Valtchanov, I., Kuneva, I., & Dissanska, M. 2005, MNRAS, 359, 1491
Krywult, J., MacGillivray, H. T., & Flin, P. 1999, A&A, 351, 883
Ledlow, M. J., Voges, W., Owen, F. N., & Burns, J. O. 2003, AJ, 126, 2740
Li, L.-X. 1998, Gen. Relativ. Gravitation, 30, 497
Materne, J., & Hopp, U. 1983, A&A, 124, L13
Maurogordato, S., Proust, D., Cappi, A., Slezak, E., & Martin, J. M. 1997, A&AS, 123, 411
Mazure, A., et al. 1996, A&A, 310, 31
Oegerle, W. R., & Hill, J. M. 1992, AJ, 104, 2078
———. 2001, AJ, 122, 2858
Pawl, A., Evrard, A. E., & Dupke, R. A. 2005, ApJ, 631, 773
Pinkney, J., Roettiger, K., Burns, J. O., & Bird, C. M. 1996, ApJS, 104, 1
Popesso, P., Biviano, A., Böhringer, H., Romaniello, M., & Voges, W. 2005, A&A, 433, 431
Porter, S. C., & Raychaudhury, S. 2005, MNRAS, 364, 1387
Quintana, H., & Melnick, J. 1982, AJ, 87, 972
Ricker, P. M. 1998, ApJ, 496, 670
Ricker, P. M., & Sarazin, C. L. 2001, ApJ, 561, 621
Roettiger, K., & Flores, R. 2000, ApJ, 538, 92
Stoughton, C., et al. 2002, AJ, 123, 485 (erratum 123, 3487)
Takizawa, M. 2000, ApJ, 532, 183
Teague, P. F., Carter, D., & Gray, P. M. 1990, ApJS, 72, 715
Trumpler, R. J., & Weaver, H. F. 1953, Statistical Astronomy (Berkeley: Univ. California Press)
York, D. G., et al. 2000, AJ, 120, 1579